SAND2016-5554C

EXPERIMENTAL AND COMPUTATIONAL INVESTIGATIONS INTO THE EFFECT OF PROCESS INDUCED STRESSES ON THE MODE I FRACTURE TOUGHNESS OF COMPOSITE MATERIALS

Stacy M. Nelson, Brian T. Werner, and James W. Foulk

Sandia National Laboratories

Livermore, CA 94551-0969

ABSTRACT

Process induced residual stresses commonly occur in composite structures composed of dissimilar materials. These residual stresses form due to differences in the composite materials' coefficients of thermal expansion as well as the cure shrinkage exhibited by polymer matrix materials. These residual stresses can have a profound effect on the measured performance of a loaded composite structure. A material property of particular interest when modeling the formation of damage in composite materials is the mode I fracture toughness. Currently, the standard method of measuring the mode I fracture toughness involves a double cantilever beam (DCB) experiment, where a pre-crack is introduced into a laminate and subsequently opened under tension. The resulting apparent fracture toughness from the DCB experiment may depend upon a coupled interaction between a material property, the mode I energy release rate, and the effect of residual stresses. Therefore, in this study, a series of DCB experiments are completed in conjunction with the solution of representative finite element models to quantify and understand the effect of process-induced residual stresses and temperature variations on the experimentally measured mode I fracture toughness. Specifically, double cantilever beam experiments are completed at three temperatures to characterize three types of specimens composed of carbon fiber/epoxy and glass fiber/epoxy materials: carbon bonded to carbon, glass bonded to glass, and carbon bonded to glass. The carbon-to-carbon and glass-to-glass specimens provide estimates of the composite's fracture toughness in the absence of significant residual stresses and the carbon-to-glass specimens indicate the effect of measurable process induced stresses. Upon completion of testing, the measured results and observations are used to develop high-fidelity finite element models simulating the residual stresses formed throughout the manufacturing process and the subsequent DCB testing of a laminate composed of the carbon/epoxy and glass/epoxy materials. The stress fields and delamination behavior predicted through simulation assist in understanding the trends observed during the DCB experiments and demonstrate the important relationship between experimental and computational efforts.

1. INTRODUCTION

Computer simulations can be useful in understanding the physical behaviors observed for loaded composite structures. Once verified for numerical accuracy, high-fidelity finite element models can be used to discern both the individual effects and effective relationships that different physical phenomena have on globally observed experimental behaviors. Recently, observations

Sandia National Laboratories is a multi-program laboratory managed and operated by Sandia Corporation, a wholly owned subsidiary of Lockheed Martin Corporation, for the U.S. Department of Energy's National Nuclear Security Administration under contract DE-AC04-94AL85000.

have been made regarding the effect of thermal residual stresses on the mode I fracture toughness of composite double-cantilever beam (DCB) specimens composed of materials exhibiting different coefficients of thermal expansion (CTEs). Specifically, it was observed that by increasing a specimen's residual stress state, through the application of progressively larger thermal excursions from the matrix material's stress-free temperature, the measured apparent fracture toughness could be significantly improved. While it has been postulated that this trend could be related to such phenomena as a rise in mode mixity due to the increasing residual stresses or possibly thermal contraction of the adhesive bondline itself, it is difficult to experimentally determine the accuracy of such claims. Therefore, this represents an opportunity for modeling and simulation to support the understanding of an experimentally observed trend.

Before modeling methods can be developed to simulate the effect of residual stresses on a composite DCB's measured toughness, a finer understanding of both the documented effects of residual stresses on fracture behavior as well as existing approaches for modeling the formation of residual stresses in composite structures is necessary. Firstly, many examples exist in literature discussing the potential effects that residual stresses may have on adhesively bonded composite structures. Both Yokozeki, et, al., and Nairn, et. al., present discussions of apparent versus true fracture toughness measurements. The authors suggest that the toughness measured from DCB specimens exhibiting residual stresses is only an apparent property and that the true fracture toughness is constant and the measurement's dependence on temperature is the result of the experiment capturing the release of stored strain energy within the adherends, in the form of beam curvature, that is induced by residual stresses. They suggest a straightforward summation of the true strain energy release rate due to crack area formation and the release of the stored strain energy to explain the increase in apparent fracture toughness with increasing residual stress [1-2].

Next, regarding the accurate simulation of the residual stresses formed in composite structures, multiple modeling methodologies were found in literature. Both Hahn, et. al., and Tavakol, et. al., present highly detailed approaches incorporating most of the relevant physics, including cure kinetics, polymer shrinkage, thermal strains, the effect of the tool-to-part interface, and the evolution of mechanical properties functionally dependent upon the cure state [3-5]. Alternatively, Jumbo, et. al., and Hanson, et. al., present a simplified approach in which a composite's processing details are accounted for through the experimental determination of the stress free temperature [6-7]. The residual stresses formed during these simple simulations are based only upon CTE differentials and temperature excursions from the stress-free condition. Regardless of model fidelity, the predictions associated with both the complex and simple approaches were well validated experimentally.

Existing literature has shown that residual stresses must be understood in the process of measuring a composite's mode I fracture toughness and, as recent research as shown, finite element methods can be implemented to accurately predict the formation of these stresses. Therefore, the objective of this study is to apply computer simulations to aid in understanding the experimentally observed trend that apparent fracture toughness will increase with increasing thermal residual stresses. Specifically, finite element models will be developed in which a residual stress state will be resolved through the application of the modeling methodology presented by Hanson, et. al [7]. Then, the previously described postulations that the experimentally observed trend is related to a rise in mode mixity or thermal contraction of the adhesive bondline itself will be examined.

2. DCB EXPERIMENTS

2.1 Material Fabrication

Determination of the critical mode I energy release rate, G_{1c}, was performed using ASTM standard D5528, which is more commonly known as the double cantilever beam experiment (DCB) [8]. For this study three panels were fabricated from two materials, a carbon/epoxy (CFRP) 8-harness satin weave fabric prepreg and a glass/epoxy (GFRP) 8-harness satin weave prepreg. The panels consisted of GFRP bonded to GFRP, $[(0/90)_{7s}]_s$, CFRP bonded to CFRP, $[(0/90)_{4s}]_s$, and GFRP bonded to CFRP, $[(0/90)_{10s}^{glass}/(0/90)_{5s}^{carbon}]$. All three laminates were laid up to produce two symmetric beams with an equivalent bending stiffness and a Teflon strip was embedded along one edge at the warp-to-warp interface between the two beams to produce a precrack. The prepreg layup was co-cured using a standard cure schedule that has been developed for this material [9]. This produced a material with V_f of 0.60 and E_{11} of 30 GPa for the GFRP and 60 GPa for the CFRP.

The panels were cut into specimens approximately 25mm wide with the Teflon precrack at one end using a water cooled diamond tile saw. Hinges were bonded to the precracked end using two adhesives, Hysol 9430 for the room and subambient temperatures and Hysol 9394 for the elevated temperature specimens. The initial length of the precrack was approximately 38mm long. The total thicknesses of each specimen were 6.82mm for the GFRP/GFRP and 7.68 for the CFRP/CFRP bulk material DCB specimens, and 8.75mm for the GFRP/CFRP asymmetric DCB (ADCB) specimen.

2.2 Experimental Procedure

The experiments were carried out using an Instron 5989 electromechanical load frame using a 2kN load cell and an environmental chamber. The three temperatures investigated were +71ºC, +25ºC, and -54ºC. These temperatures provide a wide range of ΔT's and, with that, significantly different residual stress states in the bi-material specimens. Initial tests used a laser extensometer to track the crack opening displacement but after comparison with the stroke measurement, little error was found due to frame compliance at the low loads applied. Each specimen was tested at a constant displacement rate of 1mm/min and the temperature of the specimen was verified using a Type K thermocouple. At both elevated and subambient temperatures the specimen was held under load control to ensure that contraction or expansion of the load train did not apply any loading to the specimen upon cool down or heat up. Tests were also performed to ensure that any hot or cold air did not cause a thermal drift within the load cell itself. Once the environmental chamber reached the appropriate temperature, the specimen was allowed to soak for enough time to ensure that it was isothermal.

Crack lengths and the critical mode I energy release rate were calculated using elastic beam theory to back out the current crack length from the measured load-displacement data. For the bulk material the equations used were:

$$a = \left[\frac{\delta E b h^3}{8P} \right]^{\frac{1}{3}} \qquad [1]$$

$$G_{1c} = \frac{12P^2a^2}{Ebh^3} \quad [2]$$

For the asymmetric DCB, Brown et al., derived the beam theory solution for the crack length and critical mode I energy release rate [10]:

$$a = \left[\frac{\delta b}{16P}\left(E_1h_1^3 + E_2h_2^3\right)\right]^{\frac{1}{3}} \quad [3]$$

$$G_{1c} = \left[\frac{27\delta^2}{2b^4}\left(\frac{1}{E_1h_1^3} + \frac{1}{E_2h_2^3}\right)P^4\right]^{\frac{1}{3}} \quad [4]$$

where P = load

b = width of DCB

d = crack opening displacement

E_i = Young's modulus of material *i*

h_i = thickness of laminate *i*

2.3 Experimental Results

As discussed in the introduction, the critical mode I energy release rate was assumed to be temperature independent and the variation in apparent fracture toughness could be explained by an independent, temperature dependent residual stress term. In order to test this assumption, bulk material specimens were tested, GFRP/GFRP and CFRP/CFRP, at the three different temperatures. The results can be seen below in Figure 1:

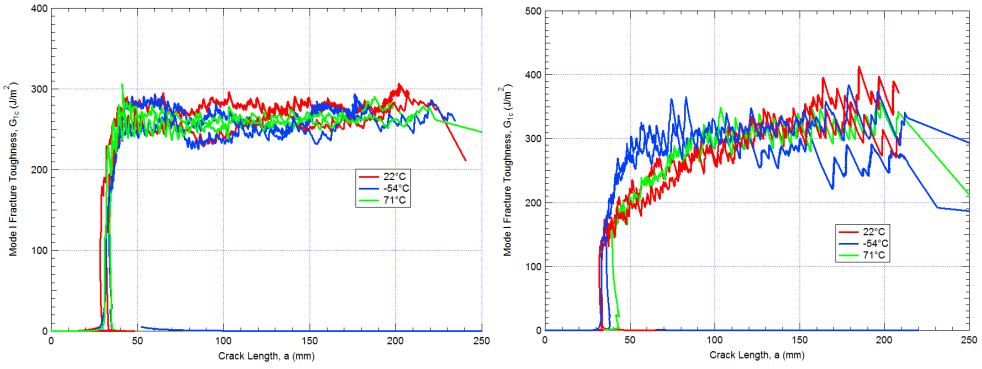

(a) (b)

Figure 1: Critical mode I energy release rate vs crack length for (a) GFRP/GFRP and (b)CFRP/CFRP laminates

Across a wide temperature range there is no apparent effect on the apparent fracture toughness. While there are residual stresses that develop at the fiber/matrix interface on the micromechanical scale, there is no CTE mismatch between the upper and lower beams on the laminate scale and thus no change in residual stress state at the interface on that length scale. This suggests that the mode I energy release rate should be temperature independent. Another observation can be made between the GFRP and CFRP laminates and that is the crack growth is much more stable in the GFRP than in the CFRP. This could be due to a combination of factors such as a smaller mismatch in stiffness between the fiber and matrix in the GFRP and smaller tows in the GFRP which produces a finer weave that creates smaller resin rich regions at the interface. These resin rich regions may provide less resistance to crack growth and thus more unstable skip-start behavior in the CFRP. The ADCB results were quite different and are shown in Figure 2 below:

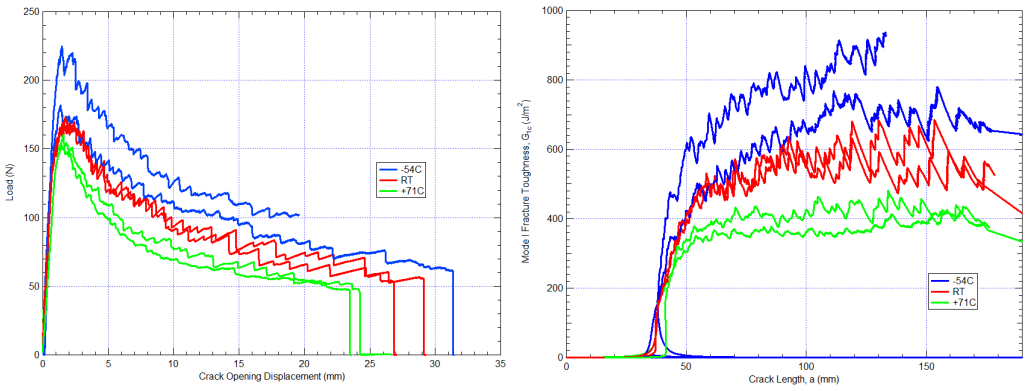

(a) (b)

Figure 2: (a) Load-displacement and (b) critical mode I energy release rate vs crack length for ADCB laminate

Unlike the bulk material DCB tests, the ADCB shows a significant temperature dependence. As the temperature drops, the ΔT increases which leads to higher residual stresses at the bi-material interface. Since higher residual stresses are correlated with higher apparent fracture toughness it is assumed that there is a complex stress state at the crack tip. With the help of computational methods, the stress fields at the crack tip can be investigated further to determine whether it is simply the residual stresses producing a stress state that is counter to the applied loading or perhaps the in-plane shear stresses along the interface are producing mixed mode behavior. It is also worth pointing out that in the bulk material DCB tests, the critical energy release rate for the GFRP was slightly under 300 J/m^2 and the CFRP is between 250 and 350 J/m^2. However, in the ADCB tests, the elevated temperature, least tough experiment showed a critical energy release rate of around 400 J/m^2, higher than that of any of the bulk material tests. This further suggests that the small amount of residual stress even at elevated temperature is beneficial to the crack propagation resistance.

3. COMPUTATIONAL METHODS

As presented in the previous section, the formation of residual stresses improved the measured

fracture toughness only in the carbon-glass DCB specimens. This implies that the observed trend is related to the formation of residual stresses, rather than some temperature dependency in the material properties. Therefore, computational methods were developed to simulate the effect of residual stress formation within the carbon-glass DCB specimens to better understand the bondline's stress evolution, the stress fields around the crack tip, and potential drivers for the increasing fracture toughness.

3.1 Description of Finite Element Model

3.1.1 Analysis Software

All simulations were completed using Sandia National Laboratories' Sierra Solid Mechanics code Adagio. Adagio is a Lagrangian, three-dimensional code for the finite element analysis of solid structures and is suitable for implicit, quasi-static analyses. Also, Sierra Adagio can make use of a multi-level solver, the solution core of which is a nonlinear, conjugate gradient algorithm that can iteratively find a solution that is within some user-defined tolerance of equilibrium. Use of the multi-level solver within Adagio aids in the solution of problems containing such challenging aspects as contact, materials with non-linear responses or extreme differences in stiffness, and material failure with element death [11].

3.1.2 Element Formulation

The modeled components were simulated with eight-noded hexahedral elements. While Sierra Adagio's default element formulation utilizes a computationally efficient, single point integration rule, avoidance of potential numerical inaccuracies common to an under-integrated element (e.g., hourglass modes) was necessary as a failure process would be modeled in these DCB simulation. Therefore, Sierra Adagio's selective deviatoric element formulation was instead applied. This element type is fully integrated with respect to the deviatoric stress response and under-integrated with respect to the hydrostatic pressure response. Also, unlike a completely fully-integrated rule, the selective deviatoric formulation does not suffer from volumetric locking [11].

Also, note that while most investigations regarding the simulation of mode I fracture toughness in DCB specimens make use of cohesive surface elements, or some other low cost crack modeling technique, the bondline in the current study was modeled with the same hexahedral elements as the composite adherends. As it has been postulated that the fracture toughness increase may in part be due to contraction of the bondline material, it was necessary to model the adhesive layer with an element capable of thermal contractions and surface elements are not able to exhibit such behaviors. To verify the assumption that the correct experimental trend could not be modeled using a traditional cohesive zone modeling approach, several preliminary simulations were completed utilizing a surface element in conjunction with cohesive models with and without mode mixing. The results of these preliminary simulations were not able to match the experimentally observed trend. Rather the cohesive zone model results imply that increasing amounts of residual stresses should decrease the experimentally measured fracture toughness and failure load. Figure 3 describes the typical results from these cohesive zone model simulations.

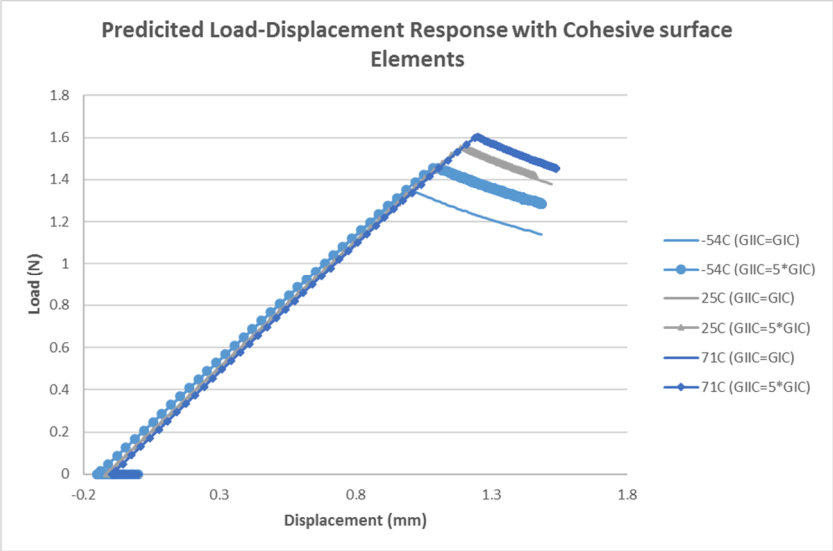

Figure 3: Sample load-displacement response predicted with cohesive zone methods

While the results shown in the above plot do not match the experimentally observed trend, they do indicate the potential importance of mode mixity. Specifically, as shown in the plot, increasing the mode II fracture toughness effectively increases the predicted peak loads for the 25ºC and -54ºC simulations. Alternatively, increasing the mode II behavior had no noticeable effect on the 71ºC predictions. This observation may indicate that large out-of-plane shear strains, that must be overcome prior to mode I fracture, form along the bondline and increase progressively with greater excursions from the stress-free temperature.

3.1.3 Material Models

The individual components of the simulated DCB geometry were modeled with three materials: the adherends were made of either the carbon or glass composite and the bondline was modeled as neat epoxy. As no yielding or failure was anticipated in either the carbon or glass adherends, these materials were simulated with Sierra Adagio's elastic-orthotropic model. This model requires the definition of the regular nine elastic constants as well as glassy and rubbery coefficients of thermal expansion in each of the materials' orthotropic directions [11]. These properties, which were determined either through experimental testing or micromechanical modeling, are listed in Table 1 for the glass and carbon composite materials.

Table 1: Material properties used to define the carbon and glass composite materials

	CFRP	GFRP
E_{11} (GPa)	63.9	24.8
E_{22} (GPa)	62.7	23.1
E_{33} (GPa)	8.6	9.7
G_{12} (GPa)	3.44	3.4
G_{13} (GPa)	3.27	2.9
G_{23} (GPa)	3.25	2.9
ν_{12}	0.048	0.13
ν_{13}	0.408	0.36
ν_{23}	0.408	0.36
CTE_{11} (rubbery) (ppm/°C)	1.14	8.31
CTE_{22} (rubbery) (ppm/°C)	1.36	9.88
CTE_{33} (rubbery) (ppm/°C)	282.9	343.5
CTE_{11} (glassy) (ppm/°C)	3.41	17.3
CTE_{22} (glassy) (ppm/°C)	3.42	17.9
CTE_{33} (glassy) (ppm/°C)	72	65.6
T_g (°C)	122.7	104.5
Stress-Free Temperature (°C)	140	140

Next, according to recommendations from literature, the bondline epoxy material was modeled with Sierra Adagio's elastic model, which requires the definition of only the material's Young's modulus, Poisson's ratio, and coefficient of thermal expansion [11]. These material parameters, which were taken from literature, are listed below in Table 2 [12-14].

Table 2: Material properties used to define the bondline adhesive

Young's Modulus (GPa)	4.0
Poisson's Ratio	0.35
CTE (ppm/°C)	45.0

Lastly, to facilitate crack growth within the modeled DCB specimen, it was necessary to define a criterion for element death within the bondline. For simplicity, and according to literature, a maximum strain failure theory was defined and executed for the previously described epoxy material. With this approach, a maximum tensile strain was defined within the adhesive layer,

and if this value was exceeded within an element, the offending element was deleted. The maximum failure strain was defined as 2.0% [12].

3.1.4 Model Geometry

The DCB experiment simulations were completed with three-dimensional geometries and meshes created using Cubit, which is a robust software toolkit capable of creating both two- and three-dimensional geometries and meshes. As described in the previous sections, since contractions within the bondline were of interest, the adhesive layer was modeled with solid elements. However, as the bondline had an average measured thickness of 0.1 mm and the carbon and glass adherends had thicknesses of 4.9 mm and 3.9 mm, respectively, geometry simplifications were necessary. In order to achieve a resolved stress state within the bondline, the adhesive layer required high quality, refined elements. Therefore, to maintain a reasonable computational cost, a plane strain model was implemented along with a truncated specimen length. Specifically, while the full 38 mm pre-crack length was modeled, the specimen's simulated bonded length was only15 mm. This simplification was deemed appropriate, as the experimentally measured fracture toughness was observed to rise to a nearly constant value after the crack grew approximately 10 to 12 mm (Figure 2). Figure 4 shows the modeled DCB geometry without meshlines.

Also, note that Sierra Adagio does not include a plane strain element. Therefore, in order to approximate the plane strain condition, the geometry shown in Figure 4 was modeled with a depth of only 1 mm and appropriate periodic boundary conditions were applied along the side surfaces of the simulated specimens. Refer to section 3.1.5 for further discussion of these approximations.

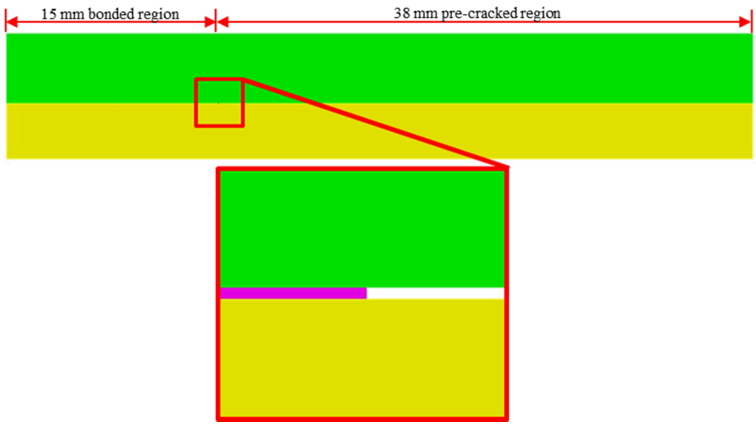

Figure 4: Representative geometry of four-point flexure simulations

3.1.5 Boundary Conditions

Boundary conditions were applied to the DCB experiment simulations to approximate the plane strain conditions as well as to emulate the formation of the thermal residual stresses and the application of the tensile, mode I loading. First, to approximate the plane strain boundary conditions, the side surfaces of the specimen were translationally fixed in the depth, or y, direction, as shown by the red arrows in Figure 5. Next, to model the formation of the thermal residual stresses before the application of the mode I loading, the process described in [7] was applied. Specifically, the DCB simulations were initiated will all components at a constant and

uniform temperature equal to the experimentally measured stress-free temperature. Then, the modeled specimens were isothermally cooled to the appropriate testing temperature (71ºC, ambient, or -54ºC); and, since the material definitions for the composite and epoxy materials included the appropriate CTE values, residual stresses were formed due to thermal contractions within the bondline and adherends. Lastly, boundary conditions were defined to mimic the mode I loading after the simulated cooling process. Namely, the bottom-front edge in the pre-cracked region was translationally fixed in the x and z directions (as shown by the blue triangles in Figure 5), while the top-front edge was translationally fixed in the x direction with an applied velocity condition applied in the vertical, or z, direction (as shown by the green arrows in Figure 5).

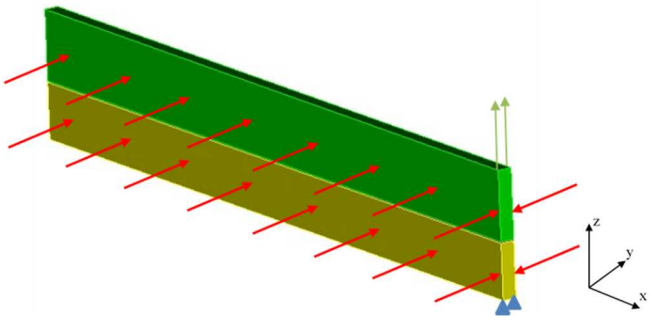

Figure 5: Description of the DCB specimen's applied boundary conditions

3.2 Mesh Convergence Study

To verify the finite element analysis methods described in the preceding sections, a grid convergence study was completed to confirm that simulated solutions were converging to the same continuum value. Furthermore, this mesh study was also used to determine the appropriate mesh size for all ensuing models. To begin this investigation, the geometry shown in Figure 5 was discretized with three different mesh sizes. The element sizes in these models were made progressively smaller through uniform refinement, as the element length within the adhesive layer was reduced from approximately 0.11 mm to 0.0556 mm to 0.04167 mm. Figure 6 shows a portion of each of the three meshed models.

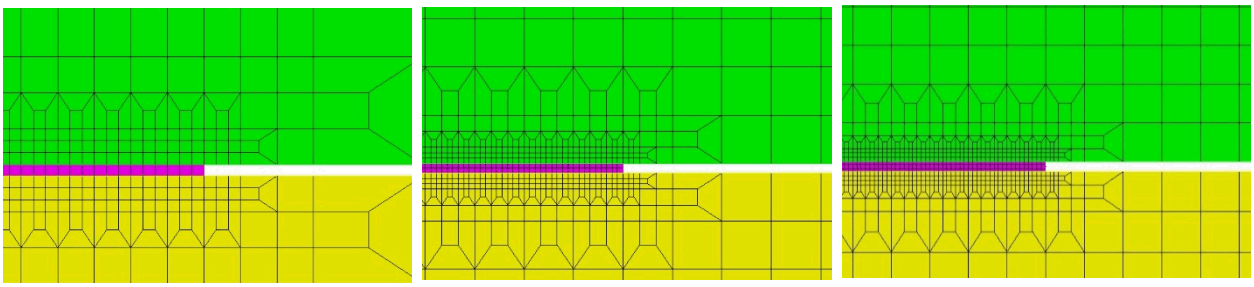

Figure 6: Three models with mesh refinement for mesh convergence study

Next, the models represented in Figure 6 were processed according to the boundary conditions described in the previous sections corresponding to a test temperature of 25ºC. Upon successful

completion of these three simulations, an estimation of the exact value, or solution corresponding to an element size of zero, of the simulated DCB experiment's peak load was determined with Richardson's Extrapolation. This method allows for the approximation of a higher order estimate of a continuum value given a series of lower order, discrete values [15-16]. Through Richardson's Extrapolation, the exact solution for this plane strain model's peak load was estimated to be 5.4 N. Figure 7 shows a plot of the percent error calculated for each grid solution as a function of mesh size and Figure 8 shows a comparison of the three simulated responses. Please note that the simulations were solved only past the point of initial load drop due to instabilities in the implicit solver related to the presence of element death and deletion.

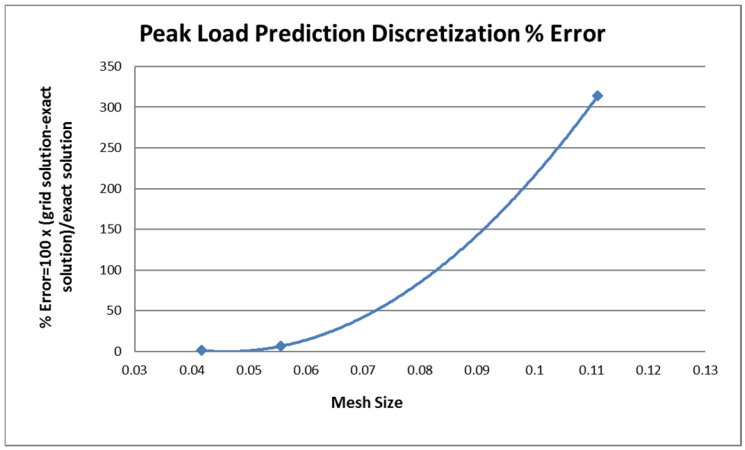

Figure 7: Error between softening loads predicted for three mesh sizes and the exact solution

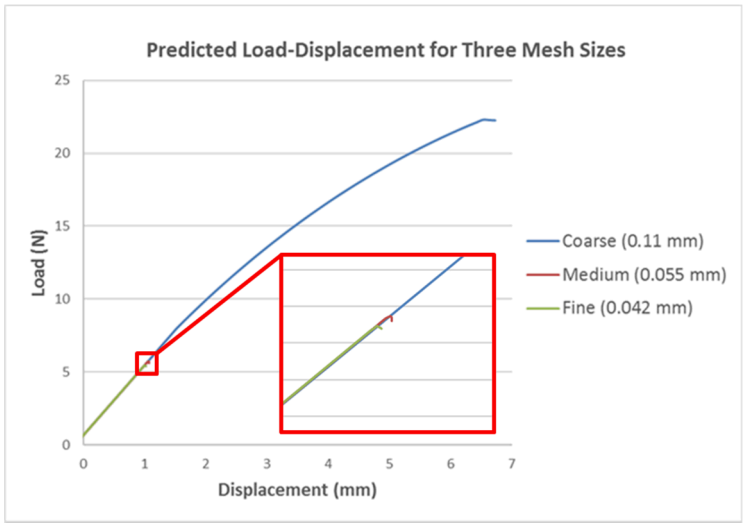

Figure 8: Simulated responses for three mesh sizes with representative displacement contour

As shown in the above plots, the percent error decreases with each level of mesh refinement, indicating that these three initial simulations are converging to the calculated exact value and lending confidence to the modeling procedure. Also, as the finest element size (0.04167 mm)

provides a discretization error less than 5%, it was chosen as the best candidate for the study's remaining models.

As an additional measure of the finest element size's validity, the normal stress along the bondline was plotted as a function of distance from the crack tip (Figure 9). According to Equation 5 from linear elastic fracture mechanics (LEFM), which can be manipulated into the form of Equation 6, if the logarithmic least squares fit of the data shown in Figure 9 takes on the form of Equation 6, the element size is sufficiently small with respect to the fracture process zone.

$$\sigma = \frac{K_I}{\sqrt{2\pi r}} \quad [5]$$

$$\log(\sigma) = -\frac{1}{2}\log(r) + \log\left(\frac{K_I}{\sqrt{2\pi}}\right) \quad [6]$$

where P = Normal stress

K_I = Mode I stress intensity factor

r = Distance from crack tip

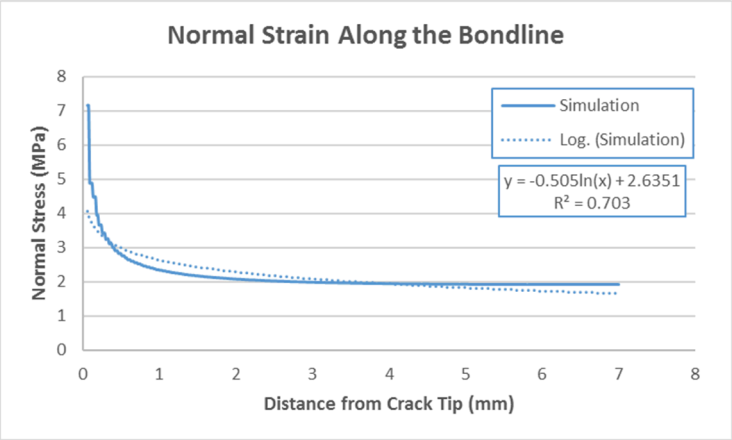

Figure 9: Logarthimic fit of normal stresses plotted along the bondline

As shown in Figure 9, the slope of the logarithmic fit is approximately -0.5. This satisfies the form of Equation 6 indicating than an element size of 0.04167 mm is sufficiently fine for this study's remaining models.

4. SIMULATION RESULTS

The computational methods described in the previous sections were developed to aid in understanding the stress evolution within the DCB's adhesive layer as well as the potential drivers for the experimentally observed fracture toughness increase. As it has been hypothesized that the measured trends are due to the residual stresses that form as a result of the CTE

differential between the composite adherends, contraction within the epoxy bondline, or a combination of these two phenomena, two types of simulations were completed. This first simulation measured the effect of just the residual stresses formed between the carbon and glass composites, while ignoring contractions within the bondline, and the second simulation included the effect of the bondline contractions.

4.1 Simulations without Bondline Contraction

With the modeling approach described in the previous sections and the converged mesh shown in Figure 6, simulations were first completed to determine the effect of the CTE differential between the carbon and glass adherends on the predicted load-displacement response. Specifically, the temperature boundary condition, described in section 3.1.5, was applied only to the composite components of the model. The adhesive layer was excluded from the thermal excursion. Figure 10 shows the load-displacement response predicted from the three different test temperatures. As with figure 8, the simulations were solved only past the point of initial load drop due to instabilities in the implicit solver related to the presence of element death and deletion.

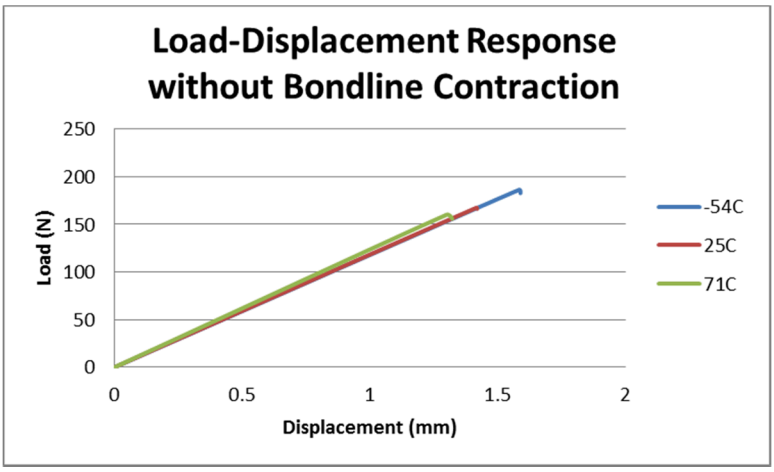

Figure 10: Predicted load-displacement responses with no bondline contraction

As shown in the above figure, the trend towards an increasing fracture toughness with increasing levels of residual stress is correctly captured. To better understand the formation of this trend, the out-of-plane shear and normal strains along the length of the plane strain model's adhesive layer were probed for each of the test temperatures after cooling and before the application of the mechanical load (Figure 11). Note that these strains were chosen to best represent the tangential (mode II) and normal (mode I) deformations within the bondline elements, which would aid in understanding the effect of mode mixity.

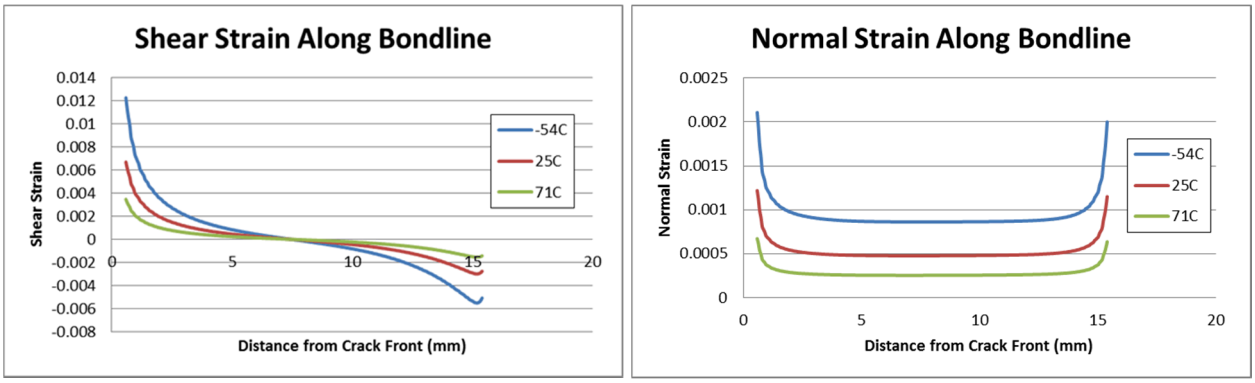

Figure 11: Shear strain (left) and normal strain (right) along the length of the adhesive layer modeled with no contractions

As shown in Figure 11, there is a sharp increase in both the shear and normal strains at the crack front as the thermal residual stresses increase. Therefore, it was hypothesized that the large shear strains deform the bondline in such a way as to counteract the mode I, tensile loading. When the mechanical loading is applied after the residual stresses are formed, the tangential deformations due to the high shear strains resist the opening of a crack and promote higher failure loads. To better visualize the evolution of the stress state at the crack front, a Mohr's circle representation of the stresses was created for each test temperature at three load levels: 0 N (after cooling and before the application of mechanical load, figure 12), 100 N (figure 13), and at the onset of failure (197 N for the -54°C model, 157 N for the 25°C model and 151N for the 71°C model, figure 14).

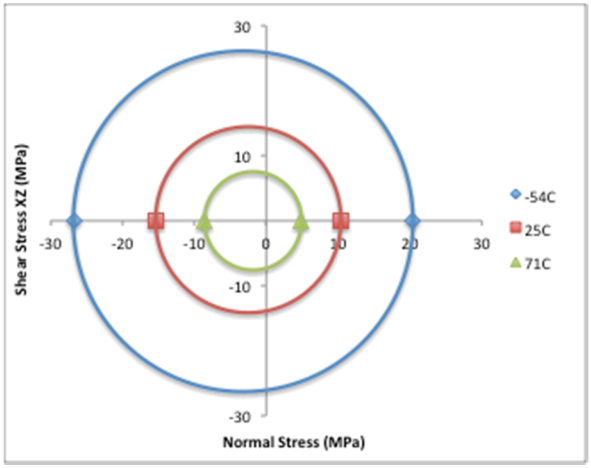

Figure 12: Mohr's circle representation of stresses at a load level of 0.0 N

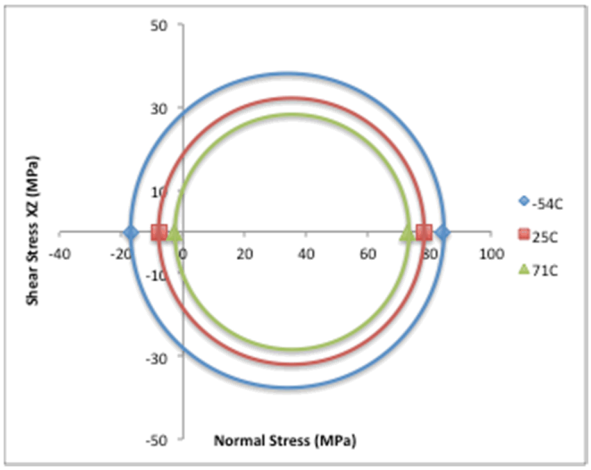

Figure 13: Mohr's circle representation of stresses at a load level of 100.0 N

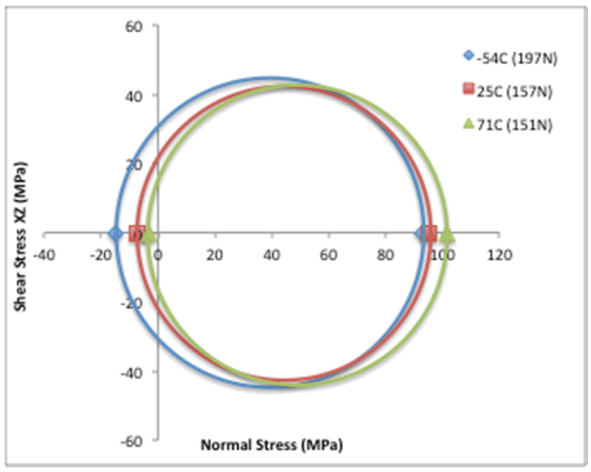

Figure 14: Mohr's circle representation of stresses at the onset of failure

As shown in Figures 12 through 14, the state of stress evolves much more quickly towards failure as the thermal residual stresses are decreased. Specifically, the rate of diametrical dilation is much greater as the test temperature increases. This lends some confidence to the assumption that the shear strains formed along the bondline as a result of cooling counteract the tensile, mode I loading and contribute to the observed experimental trends.

4.2 Simulations with bondline contractions

Next, to understand the effect of bondline contractions within the adhesive layer, the simulations described in section 4.1 were repeated with the thermal excursion applied to all model components. The predicted load-displacement responses corresponding to these three simulations are shown in Figure 15.

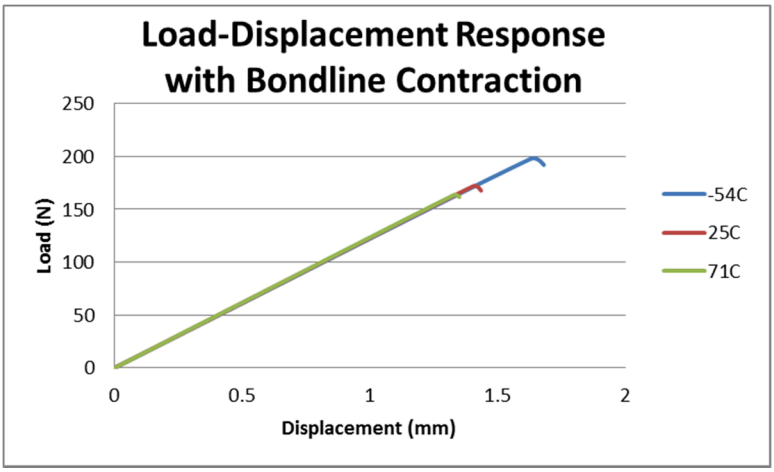

Figure 15: Predicted load-displacement responses including bondline contraction

As shown in Figure 15, the correct trend is again captured, as the predicted peak loads are progressively higher as the residual stress levels increase. Furthermore, when Figures 10 and 15 are compared, it is evident that the bondline contractions increase the predicted peak loads slightly. As with the simulations completed with no bondline contractions, the shear and normal strains along the length of the adhesive bondline were examined after the cooling phase of the simulation and, while the shear strains were not affected, the normal strains were significantly decreased (Figure 16).

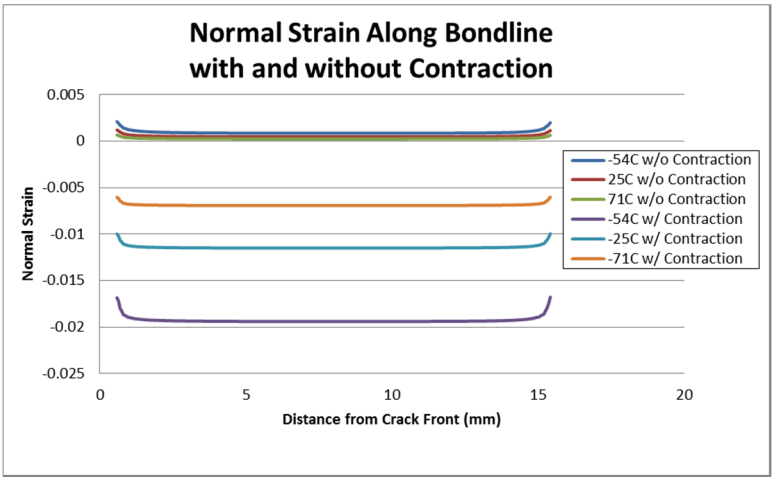

Figure 16: Comparison of the normal strain along the length of the adhesive layer modeled with and without thermal contractions

As shown in Figure 16, it is likely that the thermal contractions of the bondline place the adhesive layer in a state of compression which must be overcome by the mechanical loading, similar to the shear strain effect discussed in the preceding section. Specifically, it is likely that the combined effect of the shear strains formed due to the CTE mismatch of the composite adherends and the compressive strains resulting from the bondline's contraction result is in the

higher failure load predictions.

5. CONCLUSIONS

A modeling method was developed and implemented to promote a better understanding of the experimentally observed behavior that residual stresses enhance the mode I fracture toughness measured during the ADCB testing of a bi-material composite. Specifically, an approach utilizing solid bondline elements was executed to allow for a close examination of the stress-state evolution at the DCB specimen's crack front. The simulation results seem to indicate that the combined effect of the shear strains formed due to the CTE mismatch of the composite adherends and the compressive strains resulting from the bondline's contraction counteract the applied mechanical loads and result in higher failure predictions as the residual stress state increases. While the implemented approach is useful in understanding the drivers for the experimental trend, the computational cost of the solid bondline is prohibitive in modeling delamination is large composite structures. Ideally, the conclusions from this study will inform the development of a temperature-dependent model suitable for use with cohesive surface elements.

These results are critical to the effective use of composite materials, such as the CFRP and GFRP tested. Failure to understand the implications of residual stress on fracture toughness could lead to nonconservative designs. Using the apparent fracture toughness as an input parameter in a design that does not have the same level of residual stress could be dangerous. While one solution to this issue could be an experimental investigation in which the apparent toughness is mapped with various residual stress levels, the computational approach presented in this study has the potential for greater robustness and understanding.

6. REFERENCES

1. Yokozeki, T., Ogasawara, T., Aoki, T. "Correction Method for Evaluation of interfacial fracture toughness of DCB, ENF and MMB Specimens with Residual Thermal Stresses." *Composites Science and Technology* 68 (2008): 760-767.
2. Nairn, J. "Energy Release Rate Analysis for Adhesive and Laminate Double Cantilever Beam Specimens Emphasizing the Effect of Residual Stresses." *International Journal of Adhesion and Adhesives* 20 (2000): 59-70.
3. White, S.R., Hahn, H.T. "Process Modeling of Composite Materials: Residual Stress Development during Cure. Part I. Model Formulation." *Journal of Composite Materials* 26 (1992): 2402-2422.
4. White, S.R., Hahn, H.T. "Process Modeling of Composite Materials: Residual Stress Development during Cure. Part II. Experimental Validation." *Journal of Composite Materials* 26 (1992): 2423-2453.
5. Tavakol, B., Roozbehjavan, R., Ahmed, A., Das, R., Joven, R.m Koushyar, H., Rodriguez, A., Minaie, B. "Prediction of Residual Stresses and Distortion in Carbon Fiber-Epoxy Composite Parts Due to Curing Process Using Finite Element Analysis." *Journal of Applied Polymer Science* (2013): 941-950.
6. Jumbo, F.S., Ashcroft, I.A., Crocombe, A.D., and Abdel Wahab, M.M. "Thermal residual stress analysis of epoxy bi-material laminates and bonded joints." *International Journal of*

Adhesion & Adhesives 30(2010):523-538.

7. Hanson, A., Nelson, S., Briggs, T., Werner, B., Volk, B., Storage, T. "Experimental Measurement and Finite Element Analysis of Residual Stresses in Simple Composite Structures." *CAMX 2016*, Anaheim, CA, 2016.
8. Warnock, C., Briggs, T., "Cure Cycle Development and Qualification for Thick Section Composites", Proceedings for SAMPE 2016, Long Beach, CA, 2016.
9. ASTM D5528-13, Standard Test Method for Mode I Interlaminar Fracture Toughness of Unidirectional Fiber-Reinforced Polymer Matrix Composites, ASTM International, West Conshohocken, PA, 2013, www.astm.org
10. Brown, A. A., et al. (2013). Modeling interfacial fracture in Sierra. Livermore, CA, Sandia National Laboratories.
11. SIERRA SolidMechanics Team (2015). *SIERRA/SolidMechanics 4.38 User's Guide*, Sandia National Laboratories, Albuquerque, NM.
12. Gurusideswar, S., Velmurugan, R. "Strain Rate Dependent Behavior of Glass/Nano Clay Filled Epoxy Resin Composite," *Defense Science Journal* 64 (2014): 295-302.
13. Gurusideswar, S., Velmurugan, R., Gupta, N. "High Strain Rate Sensitivity of Epoxy/Clay Using Non-Contact Strain Measurement," *Polymer* 86 (2016): 197-207.
14. Mallick, P. *Fiber-Reinforce Composites: Materials, Manufacturing, and Design*. New York, NY: Marcel Dekker, Inc., 1993.
15. Roache, P. "Perspective: A Method for Uniform Reporting of Grid Refinement Studies." *Journal of Fluids Engineering* 116 (1994): 405-413.
16. Roache, P. "Verification of Codes and Calculations." *AIAA Journal* 36 (1998): 696-702.